

Efficient Reduced Magnetic Vector Potential Formulation for the Magnetic Field Simulation of Superconducting Magnets

Laura A. M. D'Angelo^{1,2}, Dominik Moll¹, and Herbert De Gersem^{1,2}

¹Institute for Accelerator Science and Electromagnetic Fields, Technische Universität Darmstadt, Darmstadt, Germany

²Graduate School Computational Engineering, Technische Universität Darmstadt, Darmstadt, Germany

The major advantage of reduced magnetic vector potential formulations (RMVPs) is that complicated coil structures do not need to be resolved by a computational mesh. Instead, they are modeled by thin wires, whose source field is included into the simulation model along Biot-Savart's law. Such an approach has already been successfully employed in ROXIE for the simulation of superconducting Large Hadron Collider magnets at CERN. This work presents an updated RMVP approach, which significantly outperforms the original method. The updated formulation is postulated, implemented, verified, compared to the original formulation, and applied for the simulation of a quadrupole magnet. The promising results of this work encourage further investigation towards an updated simulation framework for next-generation accelerator magnets.

Index Terms—Accelerator magnets, Biot-Savart law, finite element analysis, superconducting coils

I. INTRODUCTION

WITHOUT DOUBT, high-temperature superconducting (HTS) technology will lift next-generation synchrotrons beyond today's technological frontier [1]. With this step forward, however, magnet design is confronted with new challenges regarding the design of large, high-field and high-quality magnet systems. Computer-aided design and numerical field simulation generally play a crucial role in designing and optimizing accelerator magnet systems, and will do even more so regarding the next-generation HTS magnet systems. For the past decades, the simulation software ROXIE [2] proved to be an indispensable workhorse for designing the low-temperature superconducting (LTS) magnets of the Large Hadron Collider (LHC). ROXIE combines a hybrid finite-element (FE) boundary-element method with a reduced magnetic vector potential (RMVP) formulation [3], leading to fast and accurate simulations [4]. Herein, the coils are modeled as thin wires, and their excitation is included as a source magnetic field, which is calculated by Biot-Savart's law. The major advantage of this formulation is that these wires do not need to be resolved by a computational mesh. Especially superconducting accelerator magnets, which typically contain hundreds or thousands of coil windings, greatly benefit from this approach.

Nonetheless, ROXIE and commercial out-of-the-box simulation tools struggle with the multi-scale nature that is imposed

by HTS tapes, resulting into excessive computation times [5]. The goal of this work is to improve the computational efficiency of the RMVP approach and to contribute towards suitable simulation tools for future HTS magnet design campaigns. To do so, ROXIE's original formulation is first adapted to a pure FE model in Sec. II, and then reformulated in order to diminish the number of Biot-Savart integrals to be calculated to quantify the source magnetic field. This leads to a multi-step calculation procedure, which is presented in Sec. III and demonstrated for a case study with an eccentric line current in an iron tube. In Sec. IV, the updated RMVP formulation is analyzed regarding accuracy and performance. Herein, the proposed procedure proves to be clearly superior to ROXIE's original formulation. Sec. V finally showcases the updated RMVP formulation by applying it to the two-dimensional (2D) nonlinear magnetostatic simulation of the LHC's LTS MQXA quadrupole magnet [6]. All simulations have been carried out using the freely available FE solver GetDP [7].

II. ORIGINAL RMVP FORMULATION

In this section, the original RMVP formulation from [3] is recapitulated. The original physical problem that has to be solved is the magnetostatic problem with a homogeneous Dirichlet boundary condition, reading

$$\nabla \times (\nu \nabla \times \vec{A}) = \vec{J} \quad \text{in } V, \quad (1a)$$

$$\vec{n} \times \vec{A} = 0 \quad \text{on } \partial V. \quad (1b)$$

Herein, \vec{A} is the sought-for magnetic vector potential (MVP), ν is the reluctivity and \vec{J} is the current density, which represents the excitation in this problem. The computational domain $V = V_a \cup V_i$ consists of the coil and air domain V_a and the iron domain V_i , and ∂V is its boundary. Classically, the current excitation is modeled in the right-hand side \vec{J} , e.g. by using winding functions [8]. This procedure requires the explicit discretization of the individual wires (or at least half-turns) in the FE mesh.

In contrast, the RMVP method represents the wires by one-dimensional curves, which are not necessarily taken into account in the FE mesh. This benefits the meshing workload in the overall simulation process. The magnetic vector potential (MVP) is decomposed into

$$\vec{A} = \vec{A}_s + \vec{A}_r, \quad (2)$$

where \vec{A}_s is called the source MVP, and \vec{A}_r the reduced MVP. \vec{A}_s is obtained by evaluating Biot-Savart's law [9]

$$\vec{A}_s = \frac{\mu_0}{4\pi} \int_{\mathcal{L}'} \frac{I d\vec{s}'}{|\vec{r} - \vec{r}'|} \quad (3)$$

for *all* spatial coordinates $\vec{r} \in V$. The source domain \mathcal{L}' represents the line, on which the line current I is located. In a three-dimensional (3D) model, this would be an arbitrarily complicated curve loop in space; while in a two-dimensional (2D) setting, \mathcal{L}' is reduced to a point, which represents a line current going in or out of plane. Furthermore, in 2D, the MVP is assumed to have only a z -component, $\vec{A} = A_z(x, y)\vec{e}_z$, and Biot-Savart's law (3) becomes

$$A_z = \frac{\mu_0}{2\pi} \int_{\mathcal{L}'} I \ln(|\vec{r} - \vec{r}'|^{-1}) dr'. \quad (4)$$

Multiple sources are taken into account by superposition. Eventually, the discrete source MVP

$$\vec{A}_s(\vec{r}) \approx \sum_{j=1}^{N_{\text{edge}}} \hat{a}_{s,j} \vec{w}_j(\vec{r}) \quad (5)$$

can be computed on the mesh edges $j = 1, \dots, N_{\text{edge}}$ in two ways: One can utilize the partition-of-unity property and calculate the discrete coefficients $\hat{a}_{s,j}$ per edge e_j directly by weighting (3) with the j -th edge function \vec{w}_j and integrating over that edge e_j ,

$$\hat{a}_{s,j} = \frac{\mu_0}{4\pi} \int_{e_j} \int_{\mathcal{L}'} \frac{I d\vec{s}'}{|\vec{r} - \vec{r}'|} \cdot \vec{w}_j ds. \quad (6)$$

Alternatively, one performs a weak L^2 -projection of the Biot-Savart integral onto \vec{A}_s ,

$$(\vec{A}_s, \vec{A}'_s)_V = \left(\frac{\mu_0}{4\pi} \int_{\mathcal{L}'} \frac{I d\vec{s}'}{|\vec{r} - \vec{r}'|}, \vec{A}'_s \right)_V \quad (7)$$

with test functions $\vec{A}'_s \in H(\text{curl}; V)$ in the Hilbert space [10]

$$H(\text{curl}; V) := \{ \vec{A} \in L^2(V) : \nabla \times \vec{A} \in L^2(V) \}. \quad (8)$$

This work uses the built-in L^2 -projection of GetDP.

The reduced MVP \vec{A}_r is computed by solving the boundary value problem (BVP)

$$\nabla \times (\nu \nabla \times \vec{A}_r) = -\nabla \times (\nu \nabla \times \vec{A}_s) \quad \text{in } V_i, \quad (9a)$$

$$\nabla \times (\nu_0 \nabla \times \vec{A}_r) = 0 \quad \text{in } V_a, \quad (9b)$$

$$\vec{n} \times \vec{A}_r = -\vec{n} \times \vec{A}_s \quad \text{on } \partial V. \quad (9c)$$

Using a Ritz-Galerkin approach, the weak formulation is obtained as: Find $\vec{A}_r \in H_r(\text{curl}; V)$, s.t.

$$(\nu \nabla \times \vec{A}_r, \nabla \times \vec{A}'_r)_V = -(\nu \nabla \times \vec{A}_s, \nabla \times \vec{A}'_r)_{V_i} \quad (10)$$

$\forall \vec{A}'_r \in H_r(\text{curl}; V)$, where \vec{A}'_r is a test function, and

$$H_r(\text{curl}; V) = \{ \vec{A} \in H(\text{curl}; V) : \gamma_{\partial V}(\vec{A}) = -\vec{n} \times \vec{A}_s \} \quad (11)$$

is chosen in order to fulfill (9c). Herein,

$$\gamma_B(\vec{A}) = \vec{n} \times \vec{A}|_B \quad (12)$$

is the tangential trace operator w.r.t. a boundary B [10].

The weak formulation (10) is solved by a FE method employing standard edge shape functions. Lastly, the total MVP \vec{A} is composed of \vec{A}_s and \vec{A}_r following (2). Note that the Biot-Savart integral (3) must be evaluated in the whole domain V , whether one is actually interested in the solution of the whole domain or of only a small sub-domain.

III. UPDATED RMVP FORMULATION

A. Ansatz and Biot-Savart sub-formulation

The domain V is decomposed into a non-permeable sub-domain V_a (consisting of e.g. air) and a source-free sub-domain V_i (containing e.g. iron). Herein, V_a is fully embedded into V_i , and Γ denotes the interface between those domains. The MVP \vec{A} is then decomposed into

$$\vec{A} = \begin{cases} \vec{A}_g + \vec{A}_s + \vec{A}_m & \text{in } V_a, \\ \vec{A}_g & \text{in } V_i, \end{cases} \quad (13)$$

where \vec{A}_s is called the source MVP, \vec{A}_m the image MVP, and \vec{A}_g the reaction MVP. \vec{A}_s is obtained by evaluating Biot-Savart's law (3) for all spatial coordinates $\vec{r} \in V_a$ that are of interest, but at least for $\vec{r} \in \Gamma$. This is the major advantage to the original RMVP approach [3], where \vec{A}_s needed to be calculated in the whole domain V .

B. Image sub-formulation

The image MVP \vec{A}_m is the solution of the BVP

$$\nabla \times (\nu_0 \nabla \times \vec{A}_m) = 0 \quad \text{in } V_a, \quad (14a)$$

$$\vec{n} \times \vec{A}_m + \vec{n} \times \vec{A}_s = 0 \quad \text{on } \Gamma. \quad (14b)$$

The MVP $\vec{A}_s + \vec{A}_m$ is the equivalent of a Green's function obeying a homogeneous Dirichlet boundary condition at Γ [9]. Using a Ritz-Galerkin approach and the abbreviation $\vec{n} \times \vec{H}_m = \vec{n} \times \vec{H}'_m$ for the tangential component of the image magnetic field strength, the weak formulation is obtained as: Find $\vec{A}_m \in H(\text{curl}; V_a)$, $\vec{n} \times \vec{H}_m \in H^{-1/2}(\text{curl}; \Gamma)$, s.t.

$$(\nu_0 \nabla \times \vec{A}_m, \nabla \times \vec{A}'_m)_{V_a} + (\vec{n} \times \vec{H}_m, \vec{A}'_m)_\Gamma = 0, \quad (15a)$$

$$(\vec{A}_m, \vec{n} \times \vec{H}'_m)_\Gamma + (\vec{A}_s, \vec{n} \times \vec{H}'_m)_\Gamma = 0 \quad (15b)$$

$\forall \vec{A}'_m \in H(\text{curl}; V_a)$, $\forall \vec{n} \times \vec{H}'_m \in H^{-1/2}(\text{curl}; \Gamma)$, where \vec{A}_m is the discrete image MVP, \vec{A}'_m and $\vec{n} \times \vec{H}'_m$ are corresponding test functions, and $H^{-1/2}(\text{curl}; \Gamma)$ is a trace space [10]. Here, the boundary condition (14b) is weakly imposed by (15b), yielding a saddle-point problem [11]. In this way, the quantity $\vec{n} \times \vec{H}_m$, which will be needed for the calculation of \vec{A}_g , is already at hand. The weak sub-formulation (15) is eventually solved by a FE method employing standard edge shape functions.

C. Reaction sub-formulation

The reaction MVP \vec{A}_g is obtained by solving the BVP

$$\nabla \times (\nu \nabla \times \vec{A}_g) = \vec{J}_g \quad \text{in } V, \quad (16a)$$

$$\vec{n} \times \vec{A}_g = 0 \quad \text{on } \partial V \quad (16b)$$

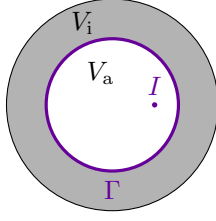


Fig. 1: 2D case study model: An infinitely long eccentric line current I in an air domain V_a surrounded by an infinitely long iron tube V_i .

with $\vec{J}_g = \vec{K}_g \delta_\Gamma$, where

$$\vec{K}_g = \vec{n} \times (\vec{H}_s + \vec{H}_m) \quad (17)$$

denotes the surface current density in A/m, and δ_Γ the delta distribution function defined by

$$\int_V f \delta_\Gamma dV = \int_\Gamma f dS \quad \forall f. \quad (18)$$

Here, $\vec{H}_s = \nu_0 \nabla \times \vec{A}_s$ and $\vec{H}_m = \nu_0 \nabla \times \vec{A}_m$ are the source and image magnetic field strengths, respectively. Visually, the current excitation in V_a has been shifted onto the interface surface Γ . The weak formulation of (16) reads:

Find $\vec{A}_g \in H_0(\text{curl}; V)$ s.t.

$$\begin{aligned} (\nu \nabla \times \vec{A}_g, \nabla \times \vec{A}'_g)_V = \\ (\vec{n} \times \vec{H}_s, \vec{A}'_g)_\Gamma + (\vec{n} \times \vec{H}_m, \vec{A}'_g)_\Gamma \end{aligned} \quad (19)$$

$\forall \vec{A}'_g \in H_0(\text{curl}; V)$, where \vec{A}'_g is a test function, and

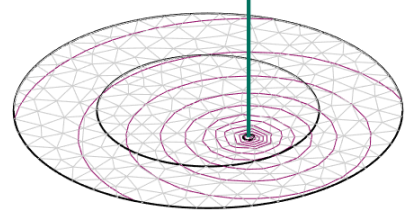
$$H_0(\text{curl}; V) = \{\vec{A} \in H(\text{curl}; V) : \gamma_{\partial V}(\vec{A}) = 0\} \quad (20)$$

is chosen in order to fulfill (16b). The weak sub-formulation (19) is solved by a FE method employing standard edge shape functions. Finally, the total MVP \vec{A} is composed of \vec{A}_g , \vec{A}_m and \vec{A}_s following (13). Note that \vec{A}_g corresponds to the full MVP in the domain V_i , which facilitates the treatment of nonlinearities and eddy currents.

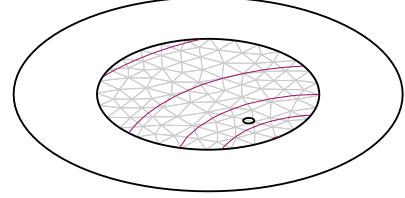
D. Case study: Eccentric line current in an iron tube

Consider as a case study an infinitely long eccentric line current I in air surrounded by an infinitely long iron tube. This model's 2D cross-section is shown in Fig. 1. V_a is defined as the air and coil region within the iron tube, while the iron tube itself is chosen as V_i . Thus, the interface Γ is the circular boundary between those two domains.

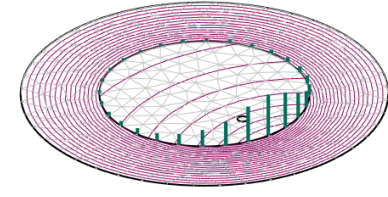
The RMVP formulation is applied to compute the MVP and magnetic flux density caused by the direct current I . Fig. 2a shows the source MVP \vec{A}_s , which is obtained by evaluating the Biot-Savart integral (3). It represents the MVP as if the eccentric line current was located in free space. The corresponding image MVP \vec{A}_m calculated by (15) is seen in Fig. 2b. Fig. 2c visualizes the surface current density \vec{K}_g determined by (17), from which the reaction MVP \vec{A}_g calculated using (19) is shown as flux lines in the same figure. The superposition of these three sub-solutions leads to the total MVP \vec{A} as shown in Fig. 2d.



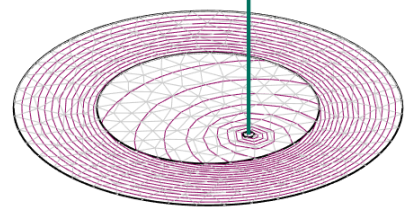
(a) Equipotential lines of the source MVP \vec{A}_s in the eccentric wire case study calculated by (3). The source current is depicted as a green line. For the sake of visualization, \vec{A}_s is calculated in the whole domain instead of only at the interface boundary.



(b) Equipotential lines of the image MVP \vec{A}_m in the eccentric wire case study calculated by (15). The computation is only done in the sub-domain V_a .



(c) The green lines visualize the surface current density \vec{J}_g at Γ determined by (17). The equipotential lines of the reaction MVP \vec{A}_g in the eccentric wire case study calculated by (19).



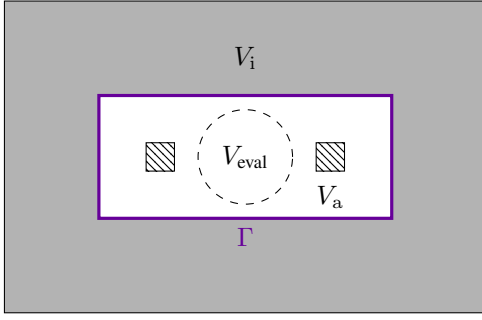
(d) Equipotential lines of the total MVP $\vec{A} = \vec{A}_s + \vec{A}_m + \vec{A}_g$ in the eccentric wire case study. The source current is depicted as a green line.

Fig. 2: The MVP components obtained in the sub-formulations of the RMVP formulation and the resulting total MVP for the case study of the eccentric wire in an iron ring.

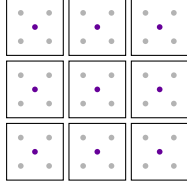
IV. NUMERICAL STUDIES

A. Benchmark model: Racetrack coil

The RMVP formulation is implemented in the freely available open-source FE solver GetDP [7] and employed to carry out a 2D linear magnetostatic simulation of a racetrack coil in an iron yoke. Fig. 3a shows the geometry, which consists of two winding groups (hatched rectangles) containing wires with rectangular cross-section and embedded in an air domain V_a (white), which is surrounded by an iron yoke V_i (gray). Γ is the interface between V_a and V_i . For the iron yoke, a linear permeability of $\mu_i = 4000\mu_0$ has been chosen. Since the line currents come together with singularities, the magnetic energy strives for infinity. Therefore, the magnetic energy considered below is evaluated in a sub-domain, which is the dashed



(a) Two coil windings (hatched rectangles, see Fig. 3b for a detailed sketch) in air (white, denoted as V_a) surrounded by an iron yoke (gray, denoted as V_i). The interface boundary between iron and air is denoted as Γ . The dashed circular domain represents the evaluation domain for the magnetic energy.



(b) Detailed view of the coil winding configuration for $N_x = N_y = 3$. In the volumetric case (1), each winding is modeled as a rectangle with a given volumetric current density. In the RMVP case (19), each half-turn is represented by a set of points (purple and gray dots) representing line currents in or out of plane, depending on the current orientation. In the simplest case, each half-turn is modeled by a single line current located in the cross-section center (purple dots).

Fig. 3: Racetrack coil model used for the purpose of numerical studies.

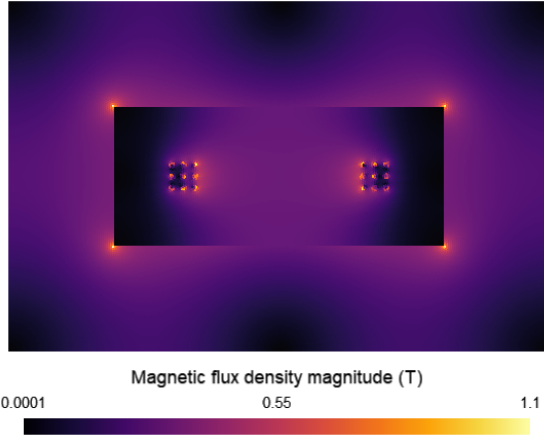


Fig. 4: Magnetic flux density magnitude in the racetrack coil obtained by the updated RMVP formulation.

circular domain V_{eval} within V_a .

The configuration of each winding group is shown in Fig. 3b. In the 2D reference model, each half-turn of the coil is modeled as a surface (black rectangles in Fig. 3b) with a given surface current density. In the 2D RMVP setting, each half-turn is discretized by a set of points (see Fig. 3b, gray and purple dots), which represent line currents in or out of plane, depending on the current orientation. In the simplest case, a half-turn is modeled by a single line current located in the cross-section center as seen in Fig. 3b (purple dots).

The results of the RMVP approach are verified against reference values obtained by a conventional 2D FE simulation modeling the half-turns as surfaces and solving (1) while

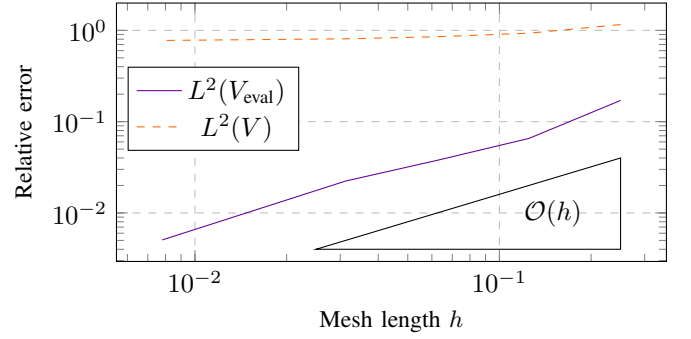


Fig. 5: Linear convergence of the L^2 -error in the evaluation domain (solid, purple) w.r.t. the mesh length for the RMVP formulation. The L^2 -error in the whole domain (dashed, orange) does not converge due to the singularities.

using a very fine mesh. The resulting magnetic flux density magnitude of the proposed method is shown in Fig. 4, where the maximal value has been capped to that of the reference solution. Particularly high fields are obtained at the four inner corners of the iron yoke due to the sharp geometry as well as the linear material properties and, of course, at the line currents due to their singular nature.

B. Convergence Analysis

For the convergence analysis, the L^2 -error w.r.t. the volumetric reference solution is considered. The line currents have to be excluded from the considered domain, as otherwise the L^2 -error would not converge due to the singularities. Therefore, a sub-domain $V_{\text{eval}} \subset V$ is chosen, such that $L' \not\subset V_{\text{eval}}$ as seen in Fig. 3a (circular region).

For lowest order FEs, one would normally expect a quadratic convergence of the L^2 -error. However, this only holds if, among other criteria, the right-hand side of the BVP is in $L^2(V)$ [12]. In the reaction sub-problem (16), the right-hand side is a Dirac source term, making the problem not regular. Although classical convergence results are therefore invalid here, it has been shown that the L_2 -error of 2D elliptic problems with Dirac source terms converges linearly [13]. Indeed, this is observed for the $L_2(V_{\text{eval}})$ -error in Fig. 5 (solid purple line).

Varying the size of V_{eval} , and thereby the remoteness of ∂V_{eval} to the line currents, neither improves nor worsens the linear convergence behavior, as long as the V_{eval} excludes the line currents or their immediate neighborhood. Then, the magnetic energy gets highly overestimated and does not converge at all (see Fig. 5, dashed orange line).

C. Performance comparison to the original formulation

The runtimes of the original and updated RMVP formulations are compared for the 2D magnetostatic linear simulation of the benchmark model with more than 100,000 degrees of freedom on a standard workstation. Both the total runtimes and the runtimes of only the Biot-Savart integral evaluation are measured. Additionally, the updated RMVP simulation is carried out for the optimal case that only the source MVP on Γ has to be computed as well as the worst case, in which the source MVP in V_a is wanted. The latter would be the case if

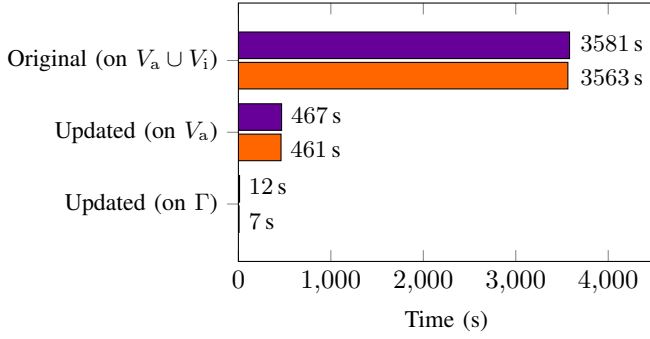


Fig. 6: Runtime comparison between the original and updated RMVP. Both the total times (purple) and the portions of the Biot-Savart integral evaluations alone (orange) are depicted. For the updated RMVP case, the worst and best case with computation of \vec{A}_s in V_a and Γ has been considered, respectively.

one is interested in the magnetic field in the whole aperture of a magnet. In practice, magnet designers are often interested in field values at particular points, e.g. in a circular curve for a multipole coefficient analysis to investigate the field quality of the magnet [14]. Therefore, the average runtime is expected to range between those two extreme cases.

Figure 6 shows the measured total runtimes (purple) and the portions of the Biot-Savart law evaluation therein (orange). The following two observations are made, from which two important conclusions are drawn:

- 1) The Biot-Savart integral computation heavily dominates the total runtime of both RMVP formulations. Therefore, the performance of the RMVP procedures can be easily and significantly improved by parallelizing the integral evaluations and employing fast-multipole methods [15].
- 2) The updated RMVP formulation is by far computationally superior to the original formulation. This holds true even for the worst case. It is even more obvious when used for the calculation of the magnetic field at particular points, along certain curves or in small-sized regions in the magnet's aperture. Then, the updated method impressively outshines the original procedure.

Hence, Fig. 6 illustrates the performance gain of the updated RMVP formulation with respect to the standard formulation and at the same time, parallelization of the Biot-Savart solver as a straightforward and promising measure for further improvement.

V. SIMULATION OF THE MQXA QUADRUPOLE

The proposed RMVP is employed to carry out a 2D magnetostatic nonlinear simulation of the MQXA low-beta quadrupole of the LHC [6] utilizing GetDP and FiQuS [16]. Each winding is approximated by one line current in its center, resulting into 488 line currents in total. Fig. 7 shows the computed magnetic flux density in the magnet. The results are compared to a reference simulation performed by a conventional 2D FE method taking the windings into account by surface current densities. Fig. 8 shows the relative difference ϵ_r of the magnetic flux density magnitude obtained by the RMVP to that of the reference simulation. As expected, high discrepancies ($\epsilon_r \geq 1$) occur in the neighborhood of the line

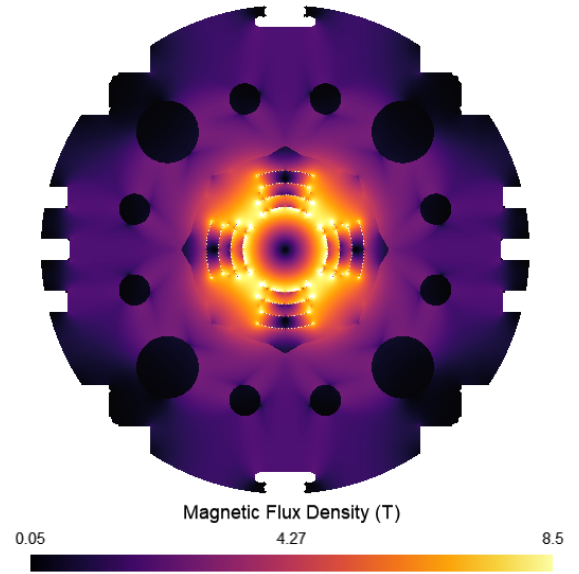


Fig. 7: Magnetic flux density magnitude in the MQXA quadrupole computed with the RMVP formulation.

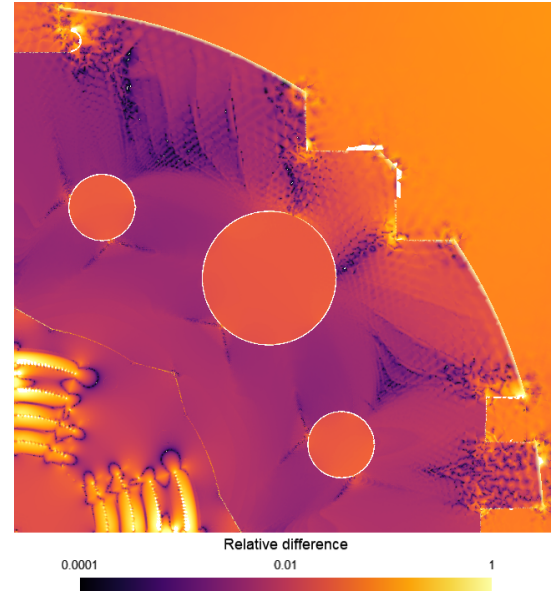


Fig. 8: Relative difference between the magnetic flux density magnitude computed by the RMVP formulation and of the reference simulation performed by a conventional 2D FE solver.

currents, which represent singularities (clearly visible in Fig. 8 as white dots). Outside the immediate neighborhood of the singularities, a good approximation is achieved with relative differences in the order of $\epsilon_r = 10^{-3}, \dots, 10^{-1}$. An even better alignment between the RMVP and reference simulation is expected if the longish winding shape was resolved by multiple line currents instead of just one at its center.

VI. CONCLUSION

This work proposed an updated RMVP formulation for accurate and fast magnetic field simulations of superconducting accelerator magnets. The formulation was postulated and verified against a benchmark model. A runtime comparison

showed that the proposed method clearly outperforms the original formulation. However, because of the Dirac source term occurring in one of the sub-problems, the L^2 -error only shows a linear convergence for lowest order FEs instead of a quadratic one. This issue is well understood in the scientific computing community, and different techniques exist to improve the convergence order [17]. Finally, the updated RMVP procedure was embedded in FiQuS, guaranteeing the greatest possible applicability in the accelerator magnet engineer community, and successfully employed to carry out a 2D nonlinear magnetostatic simulation of a quadrupole magnet.

The promising results of this work encourage an expansion of that method towards an updated simulation framework for HTS accelerator magnets, including physical formulations suitable for HTS magnets [18] and magnetization models for HTS tapes [19].

ACKNOWLEDGMENT

This work has been supported by CHART (<http://chart.ch>) in the context of the MagNum project, by the German BMBF project BMBF-05P18RDRB1, by the Graduate School Computational Engineering at TU Darmstadt, and by the DFG Research Training Group 2128 "Accelerator Science and Technology for Energy Recovering Linacs".

The authors thank Nicolas Marsic, Erik Schnaubelt, Andrea Vitrano and Bernhard Auchmann for the fruitful discussions and their helpful advice.

REFERENCES

- [1] M. Durante, F. Borgnolutti, D. Bouziat, *et al.*, "Realization and First Test Results of the EuCARD 5.4-T REBCO Dipole Magnet," *IEEE Trans. Appl. Supercond.*, vol. 28, no. 3, pp. 1–5, 2018.
- [2] S. Russenschuck, Ed., *ROXIE: Routine for the Optimization of Magnet X-Sections, Inverse Field Calculation and Coil End Design – First International ROXIE Users Meeting and Workshop*, 1998.
- [3] C. Paul, "Numerical calculation of the saturation induced field errors in the main dipole of CERN's future Large Hadron Collider," Ph.D. dissertation, Technische Universität Graz, 1997.
- [4] S. Kurz, S. Russenschuck, and N. Siegel, "Accurate calculation of fringe fields in the LHC main dipoles," *IEEE Trans. Appl. Supercond.*, vol. 10, no. 1, pp. 85–88, Mar. 2000.
- [5] F. Grilli, "Numerical Modeling of HTS Applications," *IEEE Trans. Appl. Supercond.*, vol. 26, no. 3, Apr. 2016.
- [6] R. Ostojic, "The LHC insertion magnets," *IEEE Trans. Appl. Supercond.*, vol. 12, no. 1, pp. 196–201, 2002.
- [7] P. Dular, C. Geuzaine, F. Henrotte, and W. Legros, "A general environment for the treatment of discrete problems and its application to the finite element method," *IEEE Trans. Magn.*, vol. 34, no. 5, pp. 3395–3398, Sep. 1998.
- [8] S. Schöps, H. De Gersem, and T. Weiland, "Winding functions in transient magnetoquasistatic field-circuit coupled simulations," *COMPEL*, vol. 32, no. 6, pp. 2062–2082, 2013.
- [9] J. D. Jackson, *Classical Electrodynamics*, Third ed. Hoboken, NJ, USA: John Wiley & Sons, 1998.
- [10] P. Monk, *Finite Element Methods for Maxwell's Equations* (Numerical Mathematics and Scientific Computation). New York, NY, USA: Oxford University Press, 2003.
- [11] F. Brezzi and M. Fortin, *Mixed and Hybrid Finite Element Methods*. New York, NY: Springer, 1991.
- [12] A. Ern and J.-L. Guermond, "Analysis of the edge finite element approximation of the Maxwell equations with low regularity solutions," *Comput. Math. Appl.*, vol. 75, no. 3, pp. 918–932, 2018.
- [13] R. Scott, "Finite Element Convergence for Singular Data," *Numer. Math.*, vol. 21, pp. 317–327, 1973.
- [14] S. Russenschuck, *Field Computation for Accelerator Magnets*. Weinheim: Wiley-VCH, 2010.
- [15] F. Groh, D. Beck, W. Hafla, A. Buchau, and W. M. Rucker, "Calculating Exciting Fields Using the Fast Multipole Method and an Integral Transformation to the Coil Surface," *IEEE Trans. Magn.*, vol. 41, no. 5, pp. 1384–1387, May 2005.
- [16] A. Vitrano, M. Wozniak, E. Schnaubelt, T. Mulder, E. Ravaioli, and A. Verweij, "An Open-Source Finite Element Quench Simulation Tool for Superconducting Magnets," *IEEE Trans. Appl. Supercond.*, vol. 33, no. 5, pp. 1–6, Mar. 2023.
- [17] S. Bertoluzza, A. Decoene, L. Lacouture, and S. Martin, "Local Error Estimates of the Finite Element Method for an Elliptic Problem with a Dirac Source Term," *Numer. Methods Partial Differential Eq.*, vol. 34, pp. 97–120, 2018.
- [18] L. Bortot, B. Auchmann, I. C. Garcia, *et al.*, "A Coupled A-H Formulation for Magneto-Thermal Transients in High-Temperature Superconducting Magnets," *IEEE Trans. Appl. Supercond.*, vol. 30, no. 5, Aug. 2020.
- [19] J. van Nugteren, B. van Nugteren, P. Gao, *et al.*, "Measurement and Numerical Evaluation of AC Losses in a ReBCO Roebel Cable at 4.5 K," *IEEE Trans. Appl. Supercond.*, vol. 26, no. 3, pp. 1–7, 2016.